Spontaneous fission and competing ground state decay modes of actinide and transactinide nuclei

Kanishka Sharma, Gudveen Sawhney,* and Manoj K. Sharma
School of Physics and Materials Science, Thapar University, Patiala-147004, Punjab, India
(Received 7 June 2017; revised manuscript received 26 September 2017; published 9 November 2017)

Based on the preformed cluster model, we have carried out a comprehensive theoretical study on the decay paths of ground state actinide and transactinide nuclei, specifically from ^{232}U to ^{264}Hs exhibiting the phenomenon of spontaneous fission (SF). This is an extension of our earlier studies on α decay, exotic cluster emission, and heavy particle radioactivity, where an effort is made to identify the most probable fragments in the SF process. These observations in turn, could provide a testing ground for future SF half-life measurements. To obtain a clear picture of the dynamics involved, the variations of fragmentation potential, preformation factor, and decay barrier height have been examined. The calculated potential energy surfaces show a change from a predominantly asymmetric fission to a symmetric fragmentation with the increase in the *N*/*Z* ratio of parent nuclei. In addition, an exclusive analysis of SF with α and other possible cluster emissions for the ^{232,234,236,238}U parents was made to have better insight of nuclear structure information. In other words, the comparative nature of α, cluster, heavy fragment, and SF decay paths is analyzed in view of shell closure property of the decay fragments. Interestingly, the calculated decay half-lives for the ^{82}Ge heavy cluster are in fact shown to lie within the limits of experiments, thereby presenting themselves as exciting new possibilities which may be validated via future experiments.

DOI: 10.1103/PhysRevC.96.054307

I. INTRODUCTION

Pioneering studies on various spontaneous (ground state) decays have played a leading role in understanding the nuclear phenomena and related properties. Discovery of α radioactivity was instrumental in the earlier nuclear explorations and is considered as one of the dominant decay modes of nuclei in the heavy or superheavy mass region. After about four decades from the discovery of α radioactivity, nuclear fission was discovered in 1939 [1]. Phenomenon of fission involves the division of a nucleus, with large imbalance and hence large instability, into two comparable fragments. The two radioactivities (α and β) and nuclear fission are the classical types of nuclear decays, and detailed studies of these processes provide a useful tool to understand the majority of nuclear properties. In 1980, after another four decades from the discovery of fission, it was predicted theoretically that unstable nuclei can attain stability not only by decaying via the above mentioned modes of radioactivity, but also by decaying through a very novel and exotic way, called cluster radioactivity [2,3]. Here the unstable parent nucleus is assumed to decay into a cluster, which is larger than the α particle but smaller than the lightest of fission fragments, and the daughter nucleus. Apart from this, the authors of [4,5] explored the emergence of heavy particle radioactivity (HPR) from superheavy elements (SHEs) via the spontaneous emission of heavy clusters.

Basically, all the above mentioned decay modes, i.e., α decay, cluster (both light as well heavy) emission, and fission correspond to the breakup of a nuclear liquid drop into two fragments having four different values of mass asymmetry and hence are treated as different aspects of ground state decay of nuclear systems. Various theoretical approaches [6–8] have been coined to describe the above mentioned spontaneous decays. An interesting feature of such a study is that one of the fragments always refers to spherically closed or nearly closed shell nucleus.

The first model that explained the α decay was given independently by Gamow and Gurney by applying the well-established quantum tunneling effect. It was assumed that the α particle is already formed inside the decaying nucleus and it keeps on assaulting the surface of the nucleus with certain frequency until it tunnels through the potential barrier with a certain probability. This approach for understanding the decay of nuclei forms the basis of almost all the models developed later for studying various ground state nuclear decays. Mainly there are two different types of models based on Gamow's idea. One type refers to preformed cluster models (PCMs) [9–12]. In these models, not just the α particle but all the clusters of different sizes are considered to be preformed in the mother nucleus with different probabilities depending on the mass of the parent nucleus. After this, the penetration of the barrier is similar to Gamow's penetration. In the second type of the models known as unified fission models (UFMs), the penetration is considered without bothering about the cluster being preformed or not, inside the parent nucleus. Poenaru and Greiner [13] were the first to do a theoretical calculation for cluster decay by using such criteria, naming the analytical super asymmetric fission model (ASAFM). ASAFM, in general, does not carry the relevant structure information. Alternatively, PCM contains the structure information of the decaying nucleus via the preformation factor. This approach of PCM was proved to be successful in explaining various ground state properties of the nuclei and related phenomena like cluster radioactivity, α decay, etc., in different regions of the periodic table. Knowing that the PCM calculated half-life $T_{1/2}$ is a combined effect of both preformation P_0 and penetration P probabilities, consequently the predicted half-lives remain very sensitive to the curvature and energetics of the barrier potential.

*gudveen.sahni@gmail.com

Note that the understanding of mass distributions of fissioning nuclei provide some exciting inputs regarding nuclear behavior and hence one needs to explore it on an experimental as well as theoretical front. Some experimental data [14] on spontaneous fission (SF) was assembled in past years, however, systematics of this data was not analyzed in terms of corresponding (most probable) fission fragments. In this paper, we first investigate the spontaneous decay half-lives using PCM and intend to identify the most preferred heavy fragment emissions for a variety of nuclear systems, varying from the heavy to the superheavy (SHE) mass region. Specifically, we consider ^{232,234,235,236,238}U, $^{239-241}$Pu, ^{243}Am, ^{243,245,248}Cm, ^{249}Bk, $^{249-250}$Cf, ^{253}Es, ^{250,252,254,256}Fm, ^{255,257,259}Md, ^{252,254,256,257,259}No, ^{252,253,255,256,257,259}Lr, $^{255-260}$Rf, ^{255}Db, ^{258,260,262}Sg, and ^{264}Hs nuclear systems and analyze their structural aspects in terms of behavioral patterns of fragmentation potentials. The present approach is an extension of our earlier studies [15–20] based on PCM calculations which provide reasonable agreement with the observed data on α- and cluster-decay half-lives, and hence extend an opportunity to test its validity in reference to SF dynamics of some 45 nuclei. Furthermore, a possible branching of α decay with most probable cluster decay(s) and its possible competition with (spontaneous) fission have been explored from even $^{232-238}$U parents. In other words, the comparative analysis of possible decay paths of different isotopes of U has been investigated using the collective clusterization method. In addition, various nuclear structure properties like the role of shell effects, barrier modification, and fine (or substructure) of decaying (fission) fragments have been explored. A comparison of our calculated α, cluster, and SF half-lives is made with the experimental data [14,21,22] and other available theoretical calculations [23] to emphasize the relevance and applicability of the formalism used.

Sections II and III give, respectively, the details of the preformed cluster model and the calculations for ground state decays of various actinide and transactinide nuclei. Finally, the results are summarized in Sec. IV.

II. THE PREFORMED CLUSTER-DECAY MODEL

The decay constant λ or half-life $T_{1/2}$ in PCM depends on three factors: the cluster and daughter preformation probability P_0, the barrier impinging frequency ν_0, and the barrier penetrability P,

$$\lambda = \nu_0 P_0 P, \qquad T_{1/2} = \frac{\ln 2}{\lambda}, \tag{1}$$

with ν_0 as the barrier assault frequency. The assault frequency ν_0 is given simply as

$$\nu_0 = \frac{\text{velocity}}{R_0} = \frac{\sqrt{2E_2/\mu}}{R_0}. \tag{2}$$

The impinging frequency ν_0 in this model is obtained from the experimental Q value, taken as total kinetic energy shared between the two fragments and remains nearly constant $\sim 10^{21}\text{s}^{-1}$ for all the cluster decays. Here, the preformation probability P_0 is usually calculated by solving the Schrödinger equation within the concepts of quantum mechanical fragmentation theory (QMFT) [24–28] governing the η coordinate motion at a fixed relative separation $R = R_a$, defining the first turning point of the penetration path. Considering a coupled motion in dynamical collective coordinates of mass asymmetry $\eta = (A_1 - A_2)/(A_1 + A_2)$ and relative separation R, the stationary Schrödinger equation is solved:

$$H(\eta, R)\psi(\eta, R) = E\psi(\eta, R). \tag{3}$$

P_0 contains the structure information of the decaying nucleus that enters via the fragmentation potential $V_R(\eta)$ in the Schrödinger equation, defined as

$$V_R(\eta) = -\sum_{i=1}^{2}[B(A_i, Z_i)] + \frac{Z_1 Z_2 e^2}{R} + V_P + V_\ell. \tag{4}$$

Here, B_i (i=1,2) are the binding energies of the two fragments, taken from the experimental compilation of Audi and Wapstra [29] and from the theoretical estimates of Möller *et al.* [30] whenever not available in [29]. The second term represents Coulomb interaction and V_P, V_ℓ are, respectively, the nuclear proximity potential and centrifugal potential, with the moment of inertia taken in the complete sticking limit [31,32]. Basically, the binding energies are the sum of macroscopic term V_{LDM} and δU, the empirical shell corrections. It is worth mentioning here that the present approach, i.e., Myers -Swiatecki approach does not consider deformation dependent shell corrections. As the present work is confined to spherical choice of fragmentation only, the use of the Myers-Swiatecki approach is justified. However, in recent years, the extension of microscopic corrections with inclusion of deformations was effectively studied by Gherghescu *et al.* [33,34], through the deformed two-center shell model, which describes the evolution of single particle levels from the parent potential well to that of the two-fragment potential. Apparently, the inclusion of deformations in shell correction may result in some modification in the potential depth and hence the penetration probability.

Equation (3) is solved in the decoupled approximation, $\psi^n(\eta, R) = \psi^n(\eta)\psi^n(R)$, such that the stationary Schrödinger equation for say, η motion, at a fixed R value, is

$$\left[-\frac{\hbar^2}{2\sqrt{B_{\eta\eta}}}\frac{\partial}{\partial\eta}\frac{1}{\sqrt{B_{\eta\eta}}}\frac{\partial}{\partial\eta} + V_R(\eta)\right]\psi^\nu(\eta) = E^\nu_\eta \psi^\nu(\eta). \tag{5}$$

The mass parameters $B_{\eta\eta}(\eta)$ are the classical hydrodynamical masses of Kröger and Scheid [35] used for simplicity. It is seen that this mass parameter $B_{\eta\eta}$ decreases as we move from a highly asymmetric to a symmetric choice of decaying fragments and it increases linearly with the increase in the magnitude of the neck-length parameter as depicted in Fig. 1. In principle, the shell corrected masses, like the cranking masses which depend on the underlying shell model basis, should be used. An order of magnitude for the difference introduced can be estimated by comparing the results of mass parameters calculated within the hydrodynamical and cranking-type approach [see, e.g., Fig. 2(a) in Ref. [36]]. Also, according to the works mentioned in Refs. [36–38] of the manuscript, the distance of closest approach ΔR is almost doubled and hence penetrability P gets lowered.

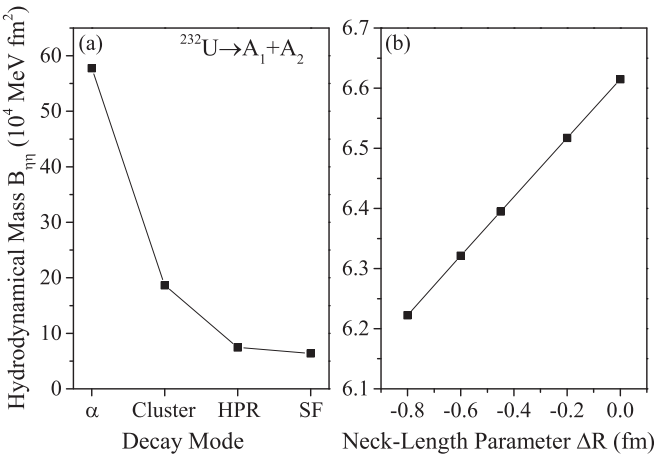

FIG. 1. The variation of hydrodynamical masses $B_{\eta\eta}$ with the (a) different decay modes and (b) neck length parameter ΔR.

Only the ground state (n=0) solution is relevant for the spontaneous fission. Then, with the properly normalized fractional cluster preformation probability P_0 at a fixed R ($=R_a$), the first turning point is

$$P_0 = |\psi[\eta(A_i)]|^2 \frac{2}{A}\sqrt{B_{\eta\eta}}. \tag{6}$$

For R motion, instead of solving the corresponding radial Schrödinger equation, the penetration probability P is estimated using WKB approximation. For the tunneling path shown in Fig. 3(c), the penetrability is expressed as

$$P = P_a W_i P_b, \tag{7}$$

$$P_a = \exp\left[-\frac{2}{\hbar}\int_{R_a}^{R_i}\{2\mu[V(R)-V(R_i)]\}^{1/2}dR\right], \tag{8}$$

$$P_b = \exp\left[-\frac{2}{\hbar}\int_{R_i}^{R_b}\{2\mu[V(R)-Q]\}^{1/2}dR\right]. \tag{9}$$

This implies that tunneling begins at $R = R_a$ and terminates at $R = R_b$ with $V(R_b)$=Q value. The de-excitation probability (W_i) between P_i and P_b is taken to be unity [39]. The only variable in our calculations is the value of first turning point $R = R_a$. In the present methodology, R_i is the effective sharp radius and is given by the expression,

$$R_i = 1.28A_i^{1/3} - 0.76 + 0.8A_i^{-1/3}. \tag{10}$$

This means that R_i depend only on A_i, i.e., $R_i(A_i)$. If we allow surface effects and define the Süssmann central radius C_i=$R_i - (1/R_i)$, we still get C_i=$C_i(A_i)$ [40]. Hence, the value of R is taken as the inner turning point $R_a = R_1 + R_2 + \Delta R(= R_t + \Delta R)$ or $= C_1 + C_2 + \Delta R(= C_t + \Delta R)$, C_i being the Süssmann central radii that assimilates to a good extent the effects of both the deformations of two fragments and neck formation between them. In the present work, two different choices of radius namely effective sharp radius R_i and Süssmann central radius C_i have been used to address half-life times of ground state fissioning nuclei. In the definition of R_a above, ΔR is the relative separation distance between two fragments or clusters A_i and is supposed to assimilate the neck formation effects and hence is referred to as the neck-length parameter. This smooth region of neck between the two spheres has its own potential [33,34]. This neck potential is constructed in such a way that it takes the same value on the necking region surface as on the ellipsoidal region surfaces of the fragments. The parameter ΔR decides the first turning point of the barrier penetration, referring to actually used barrier height and consequently to the concept of "barrier lowering" ΔV_B which simply relates $V(R_a)$ to the top of the barrier V_B as

$$\Delta V_B = V(R_a) - V_B. \tag{11}$$

It may be noted that ΔV_B reads negative as the penetration point is always below V_B, as illustrated in Fig. 3(c).

III. RESULTS AND DISCUSSIONS

The analysis of our previous study in reference to exotic cluster decay, α decay, and heavy particle radioactivity [15–19] is extended here to address the spontaneous fission in the ground state emission of various parent nuclei, so as to work out the comparative emergence of clusters and fragments of different masses, particularly the fission fragments. Note that no such fragment identification is made in the reported experiments. This section is divided into two parts. In Sec. III A, the fission half-lives of the observed spontaneous decays from ^{232}U to ^{264}Hs parents are calculated within the framework of PCM. Basically, PCM provides a better opportunity to address the ground state decays as the preformation factor gives much needed nuclear structure information. The calculations are done at temperature T=0 and a very small value of angular momentum up to $\ell = 5\hbar$ is specified particularly for neutron-rich isotopes of some parent nuclei. The behavior of the potential energy surfaces (PES), preformation profile, and barrier lowering effect, etc., are investigated to have a better understanding of the nuclear structure effects involved. Then, in Sec. III B, a comprehensive analysis is carried out to explore the different possibilities of decay modes in reference to the dynamics of even A $^{232-238}$U isotopes. Furthermore, the identification of the magic or near magic daughter is explored in the context of competing decay of SF, α-, and other cluster emission processes.

A. Spontaneous fission analysis of various mass systems ranging from heavy to superheavy region

First of all, we look at the fragmentation potentials $V(A_2)$ in Fig. 2 for the chosen ^{232}U, ^{239}Pu, ^{243}Cm, ^{250}Fm, ^{252}No, ^{252}Lr, and ^{255}Rf parents, plotted for spherical choice of fragments. Calculations are made for the optimum choice of neck-length parameters ΔR, chosen to fit the respective experimental data (see Fig. 5, explained later). It may be noted that the minima in the fragmentation potential corresponds to the maxima in the preformation probability of a particular decay mode. Here we concentrate only on the potential energy minima. For the present study, the deformation effects are not included because spherical as well as deformation effects up to β_2 do not influence the status of preferred fragment and/or hence the minima in $V(A_2)$ (for details refer to Fig. 3 of [18]). We notice two interesting results in Fig. 2: (i) Significant

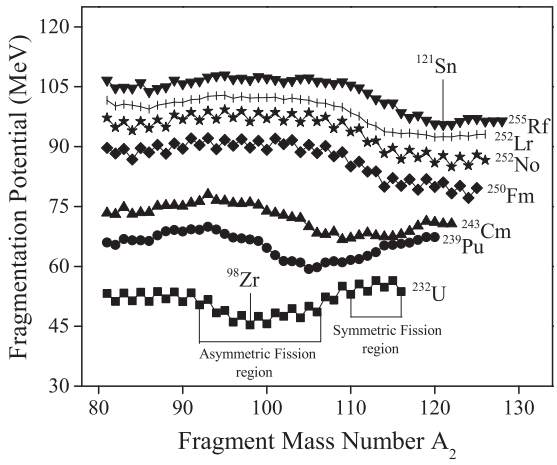

FIG. 2. Fragmentation potential $V(A_2)$ plotted for various ground state parent nuclei, taking the two emitting fragments as spheres only.

changes in the magnitude as well as in the structure of PES are observed with the increase in mass and charge number of parent nuclei which in turn would effect the relative preformation probability P_0 for all the fragments; (ii) for the lighter systems, the potential energy minima are stronger at the asymmetric fragments whereas the same are deeper for symmetric fragmentation regions for the heavier systems. For example, the PES in the case of ^{232}U nuclei clearly show that ^{98}Zr(+^{134}Te) configuration is prominent which shifts to ^{121}Sn(+^{134}Te) for the choice of the ^{255}Rf parent. A solid vertical line is drawn to point out asymmetric fragmentation and symmetric fragmentation regions. In other words, the decay of lighter ^{232}U, ^{239}Pu, and ^{243}Cm nuclei is predominantly via asymmetric fragmentation, whereas for the decays of heavier ^{250}Fm, ^{252}No, ^{252}Lr, and ^{255}Rf parents, the symmetric fragment contribution becomes dominant, compared to the asymmetric one. Such differences in the fission valley structure indicate the presence of a fine structure or substructure of fission fragments.

We have investigated the characteristics of the fragmentation path for some 45 cases of spontaneously fissioning nuclei, listed in Table I covering the majority of nuclei in the actinide and transactinide regions. Note that the fragments in the range $A_2 = 98$–130 (plus complementary heavy fragments) seem to be the prominent contributors toward SF half-lives for all the chosen fragmentation paths corresponding to ^{232}U-^{264}Hs systems, although symmetric fragments contribute more in the heavier mass region contrary to asymmetric fragmentation in lighter nuclei. Table I shows the results of our PCM-based half-lives for the chosen nuclei calculated using two different choices of radius, namely effective sharp radius R_t and Süssmann's central radius C_t, compared with available experimental data [14] (also illustrated in Fig. 6) and other model calculations [23]. The Q values are also listed in the table, calculated by using the binding energy table of [29] and, wherever not available, the theoretical values of [30] are used. The preference for the decay channel is clearly based on the minima in the fragmentation potential and hence for the cases of the largest preformation factors P_0, illustrated as an example for the ^{106}Mo fragment emitted from the ^{238}U parent in Fig. 3. The choice of different neck's ΔR for different nuclei (and hence different decay channels) suggest their occurrence at different time scales. For the majority of the chosen nuclei, the PCM calculated $T_{1/2}$ values fit the data nicely within one parameter fit of ΔR chosen in reference to the effective sharp radius $(R_t + \Delta R)$ approach. However, the same doesn't work reasonably well for neutron-rich isotopes having heavier masses. It is relevant to mention here that the potential corresponding to the first turning point $V(R_a)$ should lie within the dimensions of barrier to exercise the penetration process. However, at smaller neck values, the behavior of $V(R_a)$ was not found to be consistent with respect to the above observation and hence the deviation indicates

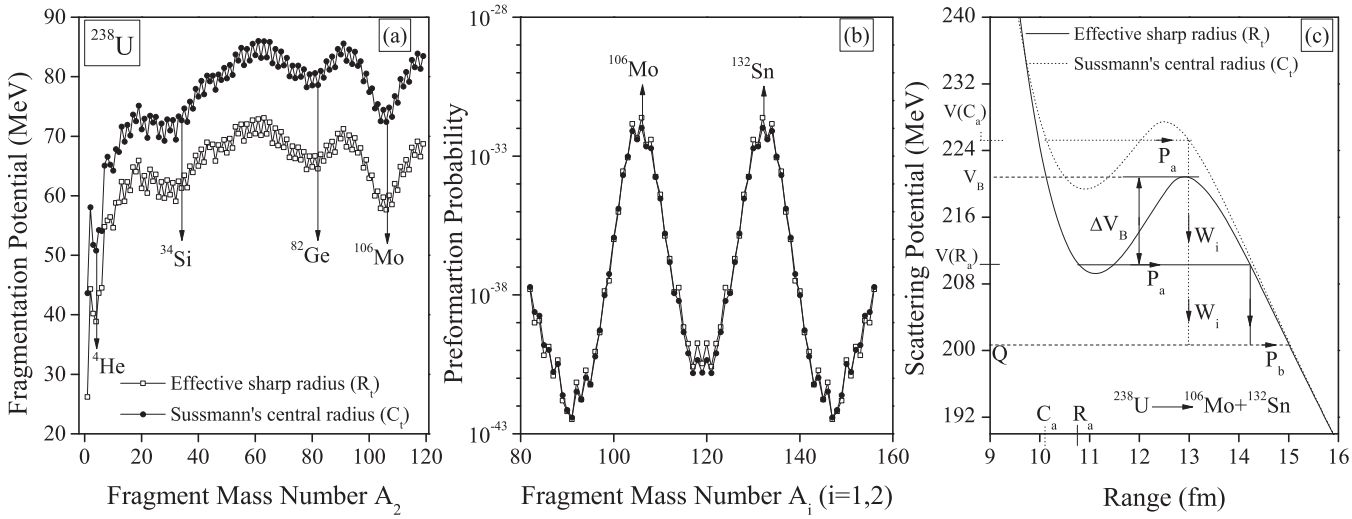

FIG. 3. (a) The variation of fragmentation potential as a function of fragment mass A_2 for the decay of ^{238}U using two different radius (effective sharp radius R_t and Süssmann's central radius C_t) approaches. (b) Same as panel (a) but for the fragment preformation probability. (c) Scattering potentials for the spontaneous decay of ^{238}U→^{106}Mo+^{132}Sn using R_t and C_t, showing the three steps of barrier penetration used in PCM.

TABLE I. Calculated half-life times compared with experimental data and other characteristic quantities like barrier lowering parameter ΔV_B, etc., for spontaneous fission of various parent nuclei to the ground states of their respective daughter nuclei. The calculations are done at $R_a = R_t \pm \Delta R$ or $C_t \pm \Delta R$ where the neck length parameter ΔR values are shown in Fig. 5.

Case	Parent	Decay	Choice of	ΔV_B	$\log T_{1/2}(s)$			Q value
No.	nucleus	channel	radius	(MeV)	PCM	GLDM [23]	Expt. [14]	(MeV)
1	^{232}U	^{98}Zr + ^{134}Te	R_t	−11.061	21.54	20.51	21.39	199.24
2	^{234}U	^{100}Zr + ^{134}Te	R_t	−10.342	23.62	22.46	23.67	199.35
3	^{235}U	^{101}Zr + ^{134}Te	R_t	−8.947	26.63	24.0	26.49	198.77
4	^{236}U	^{102}Zr + ^{134}Te	R_t	−9.643	23.85	21.74	23.89	198.97
5	^{238}U	^{106}Mo + ^{132}Sn	R_t	−9.988	23.31	21.04	23.41	200.70
6	^{239}Pu	^{105}Mo + ^{134}Te	R_t	−9.38	23.21	22.43	23.39	210.04
7	^{240}Pu	^{106}Mo + ^{134}Te	R_t	−10.549	18.13	22.7	18.17	210.26
8	^{241}Pu	^{107}Mo + ^{134}Te	R_t	−8.38	24.65	22.81	24.36	209.53
9	^{243}Am	^{110}Ru + ^{133}Sb	R_t	−8.289	21.80	20.83	21.79	215.90
10	^{243}Cm	^{109}Ru + ^{134}Te	R_t	−9.336	19.32	20.64	19.23	221.12
11	^{245}Cm	^{115}Pd + ^{130}Sn	R_t	−9.161	19.40	20.93	19.64	222.17
12	^{248}Cm	^{116}Pd + ^{132}Sn	R_t	−9.667	14.02	18.66	14.11	223.48
13	^{249}Bk	^{116}Pd + ^{133}Sb	R_t	−7.709	16.82	16.32	16.78	228.54
14	^{249}Cf	^{121}Cd + ^{128}Sn	R_t	−6.562	18.43	16.39	18.34	234.30
15	^{250}Cf	^{120}Cd + ^{130}Sn	R_t	−8.676	11.57	16.61	11.71	235.08
16	^{253}Es	^{125}In + ^{128}Sn	R_t	−4.127	13.26	12.41	13.30	243.34
17	^{250}Fm	^{124}Sn + ^{126}Sn	R_t	−7.789	7.38	7.65	7.41	248.51
18	^{252}Fm	^{126}Sn + ^{126}Sn	R_t	−6.88	9.62	8.20	9.60	249.15
19	^{254}Fm	^{126}Sn + ^{128}Sn	C_t	−0.583	5.58	7.71	7.27	250.78
20	^{256}Fm	^{128}Sn + ^{128}Sn	C_t	−0.781	1.18	6.23	4.00	253.08
21	^{255}Md	^{126}Sn + ^{129}Sb	C_t	−0.515	5.10	5.92	6.04	256.20
22	^{257}Md	^{126}Sn + ^{131}Sb	C_t	−0.928	1.97	5.25	6.30	258.20
23	^{259}Md	^{128}Sn + ^{131}Sb	C_t	−1.126	−1.41	3.46	3.76	259.89
24	^{252}No	^{122}Sn + ^{130}Te	R_t	−7.397	1.12	4.34	1.07	260.24
25	^{254}No	^{124}Sn + ^{130}Te	R_t	−6.994	4.57	4.70	4.47	260.57
26	^{256}No	^{124}Sn + ^{132}Te	C_t	−2.095	2.03	4.32	2.04	262.17
27	^{257}No	^{125}Sn + ^{132}Te	C_t	−1.762	3.21	4.30	3.23	262.48
28	^{259}No	^{126}Sn + ^{133}Te	C_t	−0.413	0.68	3.30	4.54	264.27
29	^{252}Lr	^{120}Sn + ^{132}I	R_t	−6.02	1.54	2.30	1.55	265.09
30	^{253}Lr	^{122}Sn + ^{131}I	R_t	−6.996	1.64	2.96	1.46	265.45
31	^{255}Lr	^{122}Sn + ^{133}I	R_t	−6.387	4.08	3.0	4.34	265.88
32	^{256}Lr	^{120}In + ^{136}Xe	R_t	−7.006	5.55	3.51	5.95	264.26
33	^{257}Lr	^{124}Sn + ^{133}I	C_t	−0.696	3.05	3.04	3.34	267.26
34	^{259}Lr	^{129}Sb + ^{130}Te	C_t	−0.363	0.594	2.53	3.76	268.86
35	^{255}Rf	^{121}Sn + ^{134}Xe	R_t	−6.505	0.51	1.32	0.50	271.52
36	^{256}Rf	^{122}Sn + ^{134}Xe	R_t	−5.824	−2.80	1.60	−2.19	272.14
37	^{257}Rf	^{122}Sn + ^{135}Xe	R_t	−6.691	2.64	1.93	2.59	272.37
38	^{258}Rf	^{124}Sn + ^{134}Xe	C_t	−3.582	−1.87	1.62	−1.85	273.04
39	^{259}Rf	^{124}Sn + ^{135}Te	C_t	−0.947	1.60	1.38	1.60	273.43
40	^{260}Rf	^{130}Te + ^{130}Te	C_t	−0.642	−1.70	0.55	−1.29	274.87
41	^{255}Db	^{120}Sn + ^{135}Cs	R_t	−6.232	−0.40	−0.45	−0.09	277.70
42	^{258}Sg	^{120}Sn + ^{138}Ba	C_t	−2.532	−2.09	−1.53	−2.28	284.11
43	^{260}Sg	^{122}Sn + ^{138}Ba	C_t	−2.371	−2.02	−2.38	−2.14	284.66
44	^{262}Sg	^{124}Sn + ^{138}Ba	C_t	−1.008	−2.78	−4.40	−2.15	283.12
45	^{264}Hs	^{126}Te + ^{138}Ba	C_t	−0.518	−4.47	−7.29	−2.79	297.61

that a relatively larger value of ΔR is required to address $T_{1/2}$ data. On the other hand, the calculated half-lives are found to underestimate the experimental SF data by a factor of ∼10 s at higher neck values, which, in turn, suggests that a different choice of radius may be required particularly to address SF of neutron-rich isotopes. Consequently, the impact of Süssmann's central radius $C_t + \Delta R$ is worked out and interestingly we were able to address the measured half-lives. Note that, for the angular momentum part of the potential, we have considered the case of $\ell = 5\hbar$, chosen in reference to the C_t approach whereas $\ell = 0\hbar$ is considered for the R_t choice. Specifically, for neutron-rich isotopes, we find that the comparison between the calculated and measured half-lives improves to a fair extent by considering ℓ effects up to $5\hbar$. Hence, this switching of

the radius choice from R_t to C_t along with the dependence of angular momentum with the increase in the number of neutrons of the parent nucleus, specifically in the SHE mass region provides an interesting case of investigation for further understanding of nuclear behavior.

We have carried out the comparison of R_t and C_t radius configurations on the respective fragmentation profile of the ^{238}U nucleus. Despite the use of different radii, our analysis of Fig. 3(a) clearly shows that ^{106}Mo is the most probable fission fragment, showing strongest minimum in PES with corresponding ^{132}Sn daughter. In other words, the status of the preferred fragment remains intact independent of the choice of radius used. Except for the change in magnitude, no noticeable change in the structural profile is observed. The above results can also be interpreted in terms of the preformation factor $P_0(A_i)$, plotted in Fig. 3(b). P_0 being a relative quantity, its calculation depends not only on the decay products but also on all other possible fragmentation of the parent nucleus. Interestingly, $P_0(A_i)$ are found to be nearly independent of the choice of radius, indicating asymmetric fission mass distribution around A_2=106 (plus complementary heavy fragments) for both the approaches. Apparently, the minima in PES and hence the maxima in preformation yield corresponds generally to a closed shell nucleus, which, in turn, provides further insight regarding the understanding of nuclear structure effects. One can clearly see from Table I (and Fig. 3) that the shell effects, in all the lighter systems resulting into asymmetric fragments, arise from the doubly closed shell ^{132}Sn or its neighboring daughter nucleus. Whereas for the heavier systems decaying via symmetric fission, this effect is mainly attributable to the magicity effect around light fragment charge Z_1=50 and spherical doubly magic around heavy fragment ^{132}Sn having charge Z_2=50 and neutron number N_2=82. Such nuclear shell structure effects play a significant role in the overall understanding of fission dynamics of the majority of the nuclear systems.

It is relevant to mention here that the fragmentation potential used in Fig. 3(a), when normalized with respect to binding energy, gives us the scattering potential, which is used to calculate the barrier penetrability. The quantum tunneling penetration probability in a dynamical investigation depends exponentially on the action integral, in which the integral contains a square root of the product of mass parameter B_{RR} and deformation energy. This exponential dependence within the quasiclassical WKB approximation suggests that this approach of the action integral containing the tensor of inertia is necessary in calculation. However, it was suggested in Ref. [41] that the use of effective mass B_{RR} is nearly similar to reduced mass for the incompressible irrotational approach. Hence, instead of using B_{RR}, we are using the reduced mass μ in the calculation of the WKB penetrability P as described in Eqs. (8) and (9) of Sec. II. Further, to see the influence of R_t and C_t on barrier characteristics, we find in Fig. 3(c) that at a fixed ΔR value, the scattering potential is significantly influenced with the use of different choices of radius. This means that the barrier height V_B as well as position R_B change considerably thereby affecting the tunneling probability. Because the calculated decay half-life $T_{1/2}$ in PCM depends on penetrability P as given by Eq. (1), and hence consequently on the choice of radius, this implies that the use of the R_t or C_t approach plays an important role in investigating the half-lives and hence the decay of a particular nuclear system.

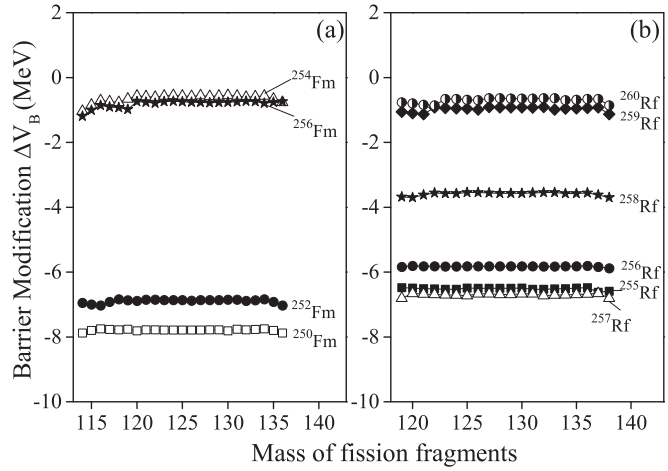

FIG. 4. Variation of barrier lowering parameter ΔV_B (MeV) with the mass of fission fragments on the x axis for (a) even $^{250-256}$Fm isotopes and (b) $^{255-260}$Rf isotopes.

Another quantity of interest is the variation of barrier modification parameter ΔV_B, plotted in Fig. 4 for various isotopes of Fm and Rf. This property of "barrier lowering" effects is a built-in property of the PCM, which has a direct dependence on the corresponding values of neck-length parameter ΔR used to fit the available data. For a given parent, the variation of ΔV_B is almost independent of the mass of fission fragment and a closer look at Fig. 4 indicates direct isospin (N/Z) dependence of ΔV_B. In other words, the magnitude of barrier modification is observed to be least for heavier isotopes, ^{256}Fm and ^{260}Rf in both the cases, and is shown to increase further with the decrease in number of neutrons of parent nuclei. However, such a systematics is not followed by ^{254}Fm and ^{257}Rf nuclei, shown, respectively, in Figs. 4(a) and 4(b), possibly because of the large variation in the observed half-life values with respect to its neighboring isotopes. This behavior of ΔV_B is found to be consistent for the majority of the systems studied here as depicted clearly in Table I.

The only parameter used in PCM is the neck length ΔR[$= R_a$-R_1-R_2 or $=R_a$-C_1-C_2], shown in Fig. 5, obtained for the best possible fit of the observed [14] SF decay half-lives data. Apart from providing information regarding the reaction time scale, a significance of ΔR lies in the fact that it decides the entry point of barrier penetration as well as the fragment's preformation. The choice of positive ΔR illustrated in Fig. 5 indicates that the entry point is shifted towards the barrier position while negative ΔR indicates that the entry level is shifted below the touching configuration R_t. We notice that the small value of ΔR is used which lies between -0.7 and 0.21 fm, i.e., $\Delta R = -0.24 \pm 0.45$ fm for all the studied spontaneous fissioning systems. This variation in ΔR could also be analyzed using polynomial fitting of degree one or two, which in turn could be used to make predictions by extrapolating or interpolating the used values of ΔR. The

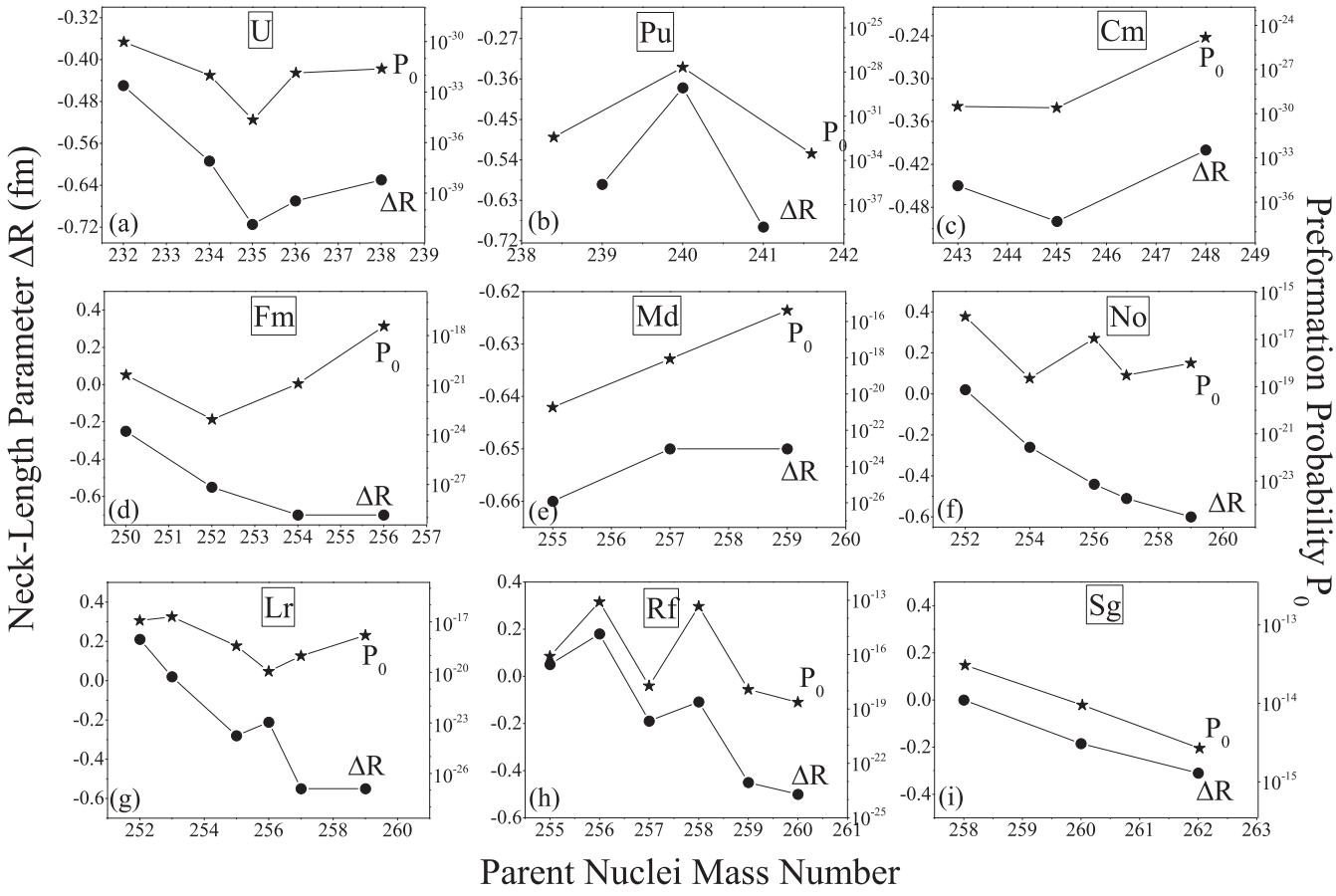

FIG. 5. The best fit neck-length parameter ΔR in fm (left Y axis) and preformation probability P_0 (right Y axis), plotted as a function of parent nuclei mass number A calculated on the basis of PCM for the most favored decays of the parents with Z=92, 94, 96, 100, 101, 102, 103, 104, and 106.

resulting information could possibly provide directions for new experiments. Similarly, the preformation probability P_0 gives us the probability of pre-born fragments prior to the decay process, and hence accounts for the structure effects of a nuclear system. The observed one to one correspondence between ΔR and P_0 for all the chosen 45 cases corresponding to different isotopes of U, Pu, Cm, Fm, Md, No, Lr, Rf, and Sg systems in Fig. 5 implies the fact that ΔR plays an important role in governing the fission dynamics involved in heavy and SHE mass regions.

As a next step, using the preformation probability P_0 and penetrability P calculated in reference to fragmentation potential $V(A_i)$ [Fig. 3(a)] and scattering potential V(r) [Fig. 3(c)], respectively, for all the chosen parent nuclei, we estimate the SF half-lives $T^{\rm SF}_{1/2}$ illustrated in Fig. 6, presented in Table I as well. The relevant comparison is made with experimental half-lives [14] and the ones computed with the WKB approximation [23]. Except for the ^{256}Fm, ^{257}Md, ^{259}Md, ^{259}No, and ^{259}Lr parents, we notice in Fig. 6 that our PCM calculated $T_{1/2}$ agree nicely with the experimental data, which, in turn, gives a confidence that this approach should impart a reasonable estimate of the most probable emitted fission fragment. Importantly, note that no such information on the individual fragments have been identified in the available [14] experiment. On the other hand, the reported PCM calculations of SF half-lives here correspond to the choice of the most preferred fragment in the SF decay of all the parent nuclei, which, in turn, could provide a testing ground for the future experiments. For the sake of comparison, we have also calculated the standard rms deviation from the experimental data using the following equation:

$$\sigma = \sqrt{\sum_{i=1}^{n}[\log_{10}(T_i/T_{\rm exp.})]^2/(n-1)}. \qquad (12)$$

The value of standard rms deviation σ comes out to be 1.958, which seems to suggest that PCM provides reasonable estimates of SF phenomenon along with the various other ground state processes analyzed earlier in previous [15–19] works.

B. Competition of α, cluster, heavy cluster, and SF decays of U isotopes.

Here, the possible decay modes of even A $^{232-238}$U parents have been explored using the collective clusterization approach. We take up this study to analyze the competition of SF (reference to Sec. III A) with α and other possible cluster emissions for the ^{232,234,236,238}U parents. Based on the availability of α-, cluster, and SF experimental half-life

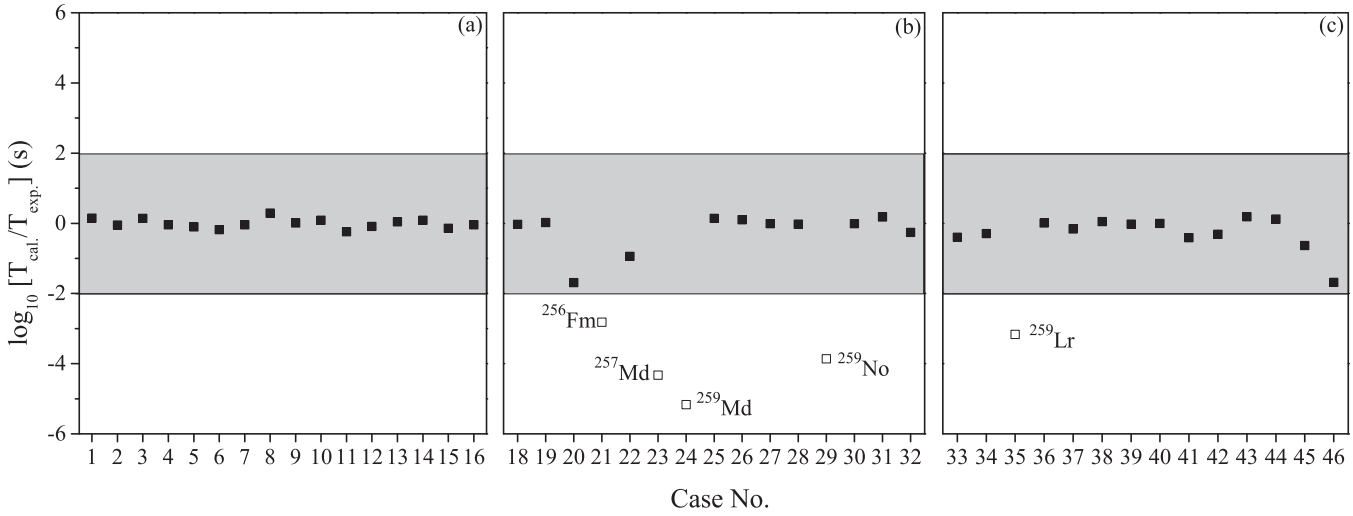

FIG. 6. Deviations between the logarithms of the PCM calculated half-lives and the experimental ones corresponding to different cases of spontaneous fissioning nuclei, mentioned in Table I.

data [14,21,22], we limit our study to only isotopes of U. We intend to carry out a comprehensive analysis of the shell closure effect of decay fragments, corresponding to different mass regions or else the isospin (N/Z ratio) effect of various mass distributions and related characteristic quantities in the decay of $^{232-238}$U isotopes.

Figure 7 shows comparative behavior of fragmentation potentials, based on Eq. (4) corresponding to different mass regions of the decaying fragments, calculated at a fixed R value for the chosen ^{232,234,236,238}U isotopes. Apart from the α's minima, we notice in Fig. 7 that in each case, there is a minimum corresponding to the cluster region [Fig. 7(b)] in addition to at least two other minima referring to heavy mass [Fig. 7(c)] and asymmetric mass fragments [Fig. 7(d)], which allow us to extract significant information regarding the structural aspects in the decay of U isotopes. The same result was analyzed earlier in Fig. 3 for ^{238}U only, though the calculated fragment preformation distribution P_0 in Fig. 3(b) was illustrated for the spontaneous fissioning region only. In addition to the α particle [Fig. 7(a)], the potential energy minima in Fig. 7(b) show a clear preference for experientally observed clusters ^{24}Ne, ^{26}Ne, ^{28}Mg, and ^{34}Si thereby suggesting the probable occurrence of possible cluster emission, respectively, from ^{232}U, ^{234}U, ^{236}U, and ^{238}U parents. Also, the emergence of heavy cluster ^{82}Ge and the corresponding daughter in Fig. 7(c) is found equally favored for all the chosen parents, which, in turn, suggest that HPR emission is competing with α- and cluster-decay processes. Note that the stability of heavy fragment ^{82}Ge can be attributed to the expected neutron magicity at N=50, which may be verified via future experiments, and may impart useful information regarding further understanding of related aspects.

In reference to the analysis of the fission region, we notice from Fig. 7(d) that the fragments in the mass range A_2= 98–106 (plus complementary heavy fragments) contribute towards SF half-lives of $^{232-238}$U nuclei, however, such identification is not exercised in experiments so far. The behavior of PES is clearly asymmetric for ^{232}U, however, the contribution of symmetric fragments starts dominating as we increase the mass of U isotopes. In other words, symmetric fragmentation is preferred for neutron-rich isotopes. These differences in the fission valley structure of fragmentation potentials or, equivalently, in preformation yields suggest the presence of a fine structure or substructure of fission fragments.

Clearly for the ^{232}U nucleus, the closed shell effects of doubly magic ^{208}Pb on ^{24}Ne, ^{134}Te on ^{98}Zr fragments are clearly depicted here in terms of strong minima in Figs. 7(b) and 7(d) of fragmentation characteristics $V(A_2)$ [or equivalently, as a shoulder in P_0, shown explicitly for ^{238}U in Fig. 3(b) for both light and heavy mass regions]. The same result holds well despite the choice of different ^{234,236,238}U parents, thereby providing much needed information regarding the structural behavior of these exotic nuclei.

Similarly, the barrier characteristics in terms of barrier height, position, and frequency are shown to be significantly influenced for the choice of different decay modes. One can clearly see in Fig. 8 that the scattering potential changes considerably for α-, cluster, heavy cluster, and SF decay paths of ^{232}U thereby affecting penetrability P, and hence the decay half-life $T_{1/2}$ as well. The barrier penetration path is also shown in the same figure. Note that the penetration between two turning points in PCM is divided into three different processes to account for the decay into the ground state of the daughter nucleus and the emitted cluster.

Next, we have investigated the dependence of the penetrability on the Q value, illustrated in Fig. 9 plotted as a function of asymmetry of daughter and cluster mass numbers. Because smaller Q value should indicate relative decrease in the penetration probability, the same is shown to be the case here. One may notice that the penetrability follows the trend of Q value and hence decreases with the increase in mass asymmetry of the decay fragments. In other words, the decay probability is strongly influenced and found to be larger for SF followed by HPR, cluster, and α-decay processes. This observation implies that the Q value of decay fragments plays a crucial role in deciding the clusterization process of nuclear systems.

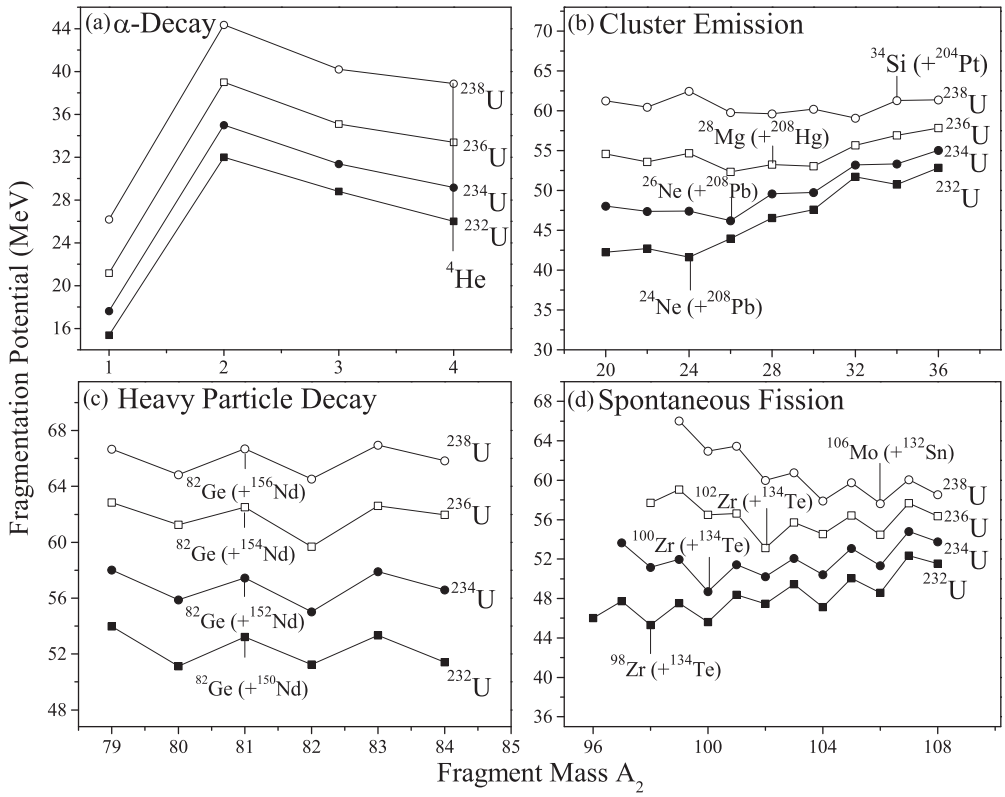

FIG. 7. Comparative behavior of fragmentation potential for even $^{232-238}$U parents for different decay paths namely (a) α radioactivity, (b) cluster emission, (c) heavy particle decay, and (d) spontaneous fission. The choice of most preferred fragments is identified by solid arrows.

The consequences of the above results, in terms of P_0 and P are shown explicitly in Fig. 10 and Table II along with the decay half-life $T_{1/2}$ for α decay, SF emission, and the most preferred clusters emitted from even $^{232-238}$U parents. The calculated half-lives in Table II are in decent agreement with experimental data for all the probable decay modes in

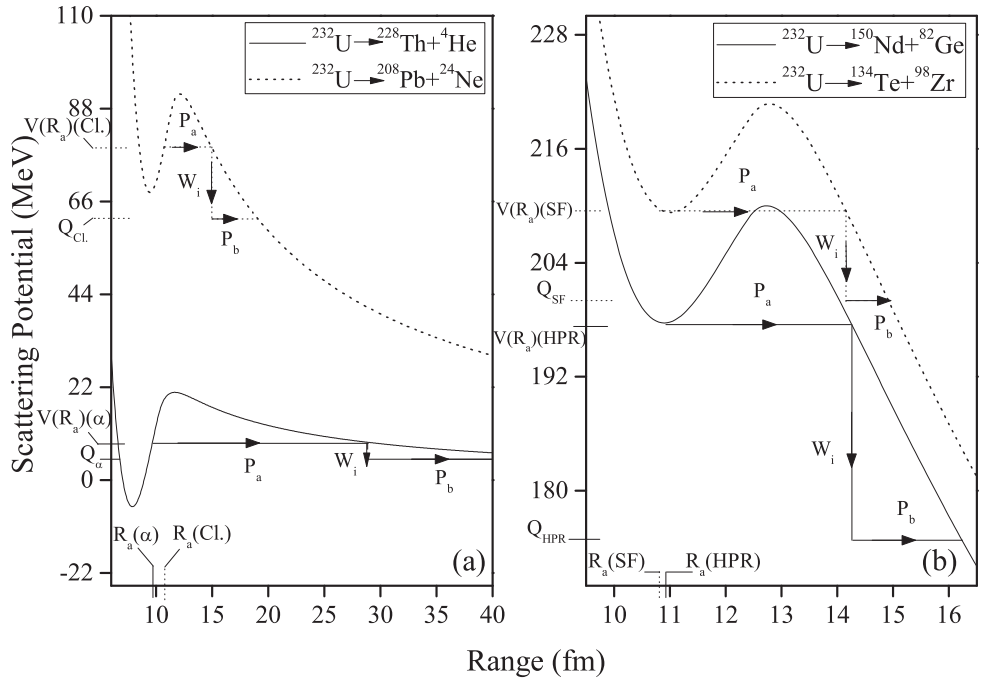

FIG. 8. The scattering potential for the four possible decay modes occurring in ^{232}U showing steps of barrier penetration with both the daughter and cluster taken as spherical only. The path of barrier tunneling is also shown.

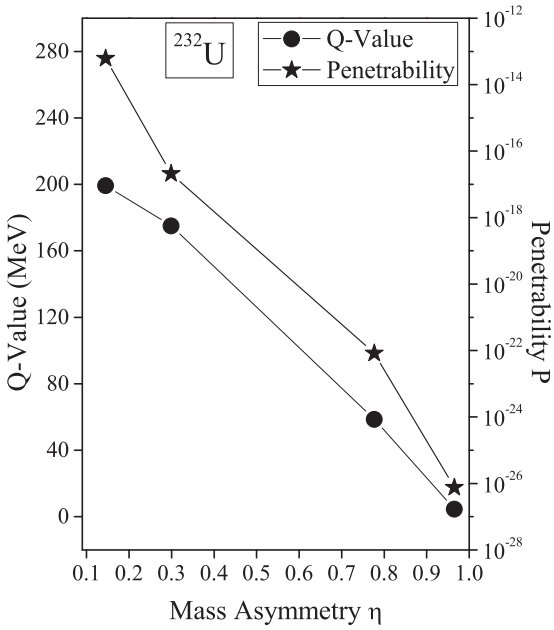

FIG. 9. Variation of Q value (MeV) (left Y axis) and penetrability P (right Y axis) with the mass asymmetry of the emitted fragments for the parent nucleus ^{232}U.

even mass $^{232-238}$U isotopes. Irrespective of the choice of parents, the measured half-lives are attained at a fixed neck value of 0.8 fm, 0.5 fm, and −0.5 fm, respectively, for α, cluster decay, and SF processes. In other words, for a given parent, the different decay products are considered to occur at different time scales and hence the use of different ΔR values seems justified. For the case of heavy cluster decays, no experimental measurement is available to date, therefore the choice of neck length (=−0.25fm) is made on the basis of assumption that ΔR for the case of HPR lies in between that for the cluster and SF decays.

Moreover, for all the considered parents, the closed shell effects of daughter or cluster seem to play a crucial role which could be of interest to investigate the ground state decays and the nuclear-structure effects related to U isotopes. The calculated decay half-lives in Fig. 10 present some interesting results: (i) ^{4}He is always preformed with the largest probability in all parents, though its corresponding P values are significantly small. Such a result is important because $T_{1/2}$ is a combined effect of both P_0 and P (ν_0 being a constant). (ii) α-decay half-life for ^{238}U is higher than for ^{232}U, ^{234}U, and ^{236}U parents, which means that the ^{238}U nucleus is more stable against α emission than others. (iii) The heavy cluster ^{82}Ge seems to be preformed with larger P_0 value, compared to ^{24}Ne, ^{26}Ne, ^{28}Mg, ^{34}Si, respectively, in ^{232}U, ^{234}U, ^{236}U, and ^{238}U parents. The calculated half-lives for ^{82}Ge heavy clusters lie within the present limits of experiments, thereby presenting themselves as further interesting cases of cluster-decay measurements. Thus, one may consider the possibility of heavy fragment in addition to α decay, cluster, or fission fragmentation of nuclear systems.

In view of the fact that fragments appearing at minima in the potential $V(\eta)$ (Fig. 7) correspond to the probable

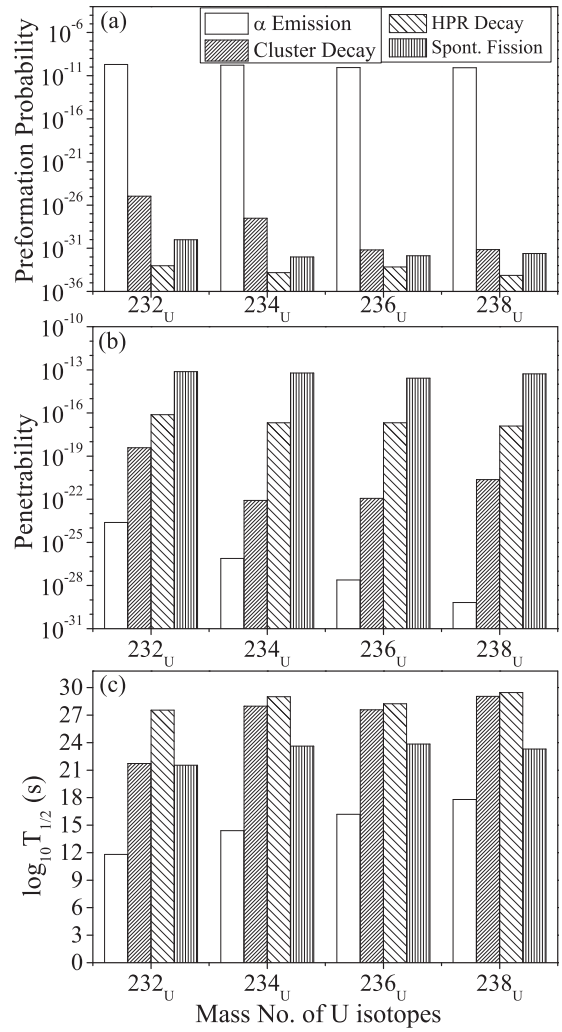

FIG. 10. Histogram representation of (a) preformation probability, (b) penetrability, and (c) logarithm of decay half-lives for the four different decay modes (α, cluster, heavy particle, and SF) of ground state parent nuclei ^{232}U, ^{234}U, ^{236}U, and ^{238}U.

configuration with respect to its neighboring clusters, an attempt has been made in Fig. 11 to analyze the Geiger-Nuttal (GN) plot for various clusters emitted from $^{232-238}$U. Some of the clusters like ^{8}Be, ^{10}Be, ^{14}C are not shown in Fig. 7 because the present calculations are directed more towards the exotic decays appearing in different mass regions of the chosen $^{232-238}$U parents. However, the same could be seen clearly preferable in terms of the minima or coming down of one cluster with respect to another, in the complete fragmentation plot shown for ^{238}U in Fig. 3(a). We notice in Fig. 11 that the $\log_{10}T_{1/2}$ vs $Q^{-1/2}$ plot for each cluster exhibits nearly a straight line but with different slopes and intercepts. In other words, the equation of the straight line (the GN law) for each cluster comes out to be different. This difference of slope and intercept for each cluster is probably associated with their different preformation P_0 and penetration factor P. Such studies could be of extreme interest in examining the cluster dynamics and its related aspects for better understanding of nuclear behavior involved in such processes.

TABLE II. PCM calculated preformation probability P_0, penetrability P, and half-life times $T_{1/2}$ for α, cluster, heavy fragment, and SF decays. The relevant comparison is made with the available data. The choice of the outgoing channel for each decay mode is based on the most probable fragment having highest preformation probability factor. Note that in each case, we refer here to calculations with $\ell = 0\hbar$ and consider a spherical choice of fragments. For best fit to α decay, cluster emission, and SF data, ΔR values are, respectively, 0.8 fm, 0.5 fm, and -0.5 fm for $^{232-238}$U whereas ΔR=-0.25 fm is chosen for heavy particle decay paths for all the U isotopes, by assuming that it lies in between that for the cluster and SF.

Decay modes	Decay channel	P_0	P	$\log_{10}T_{1/2}(s)$ PCM	Expt.
Alpha (α)	$^{232}\mathrm{U} \rightarrow {}^{4}\mathrm{He} + {}^{228}\mathrm{Th}$	1.99×10^{-10}	2.46×10^{-24}	11.81	9.34 [21]
Cluster	$^{232}\mathrm{U} \rightarrow {}^{24}\mathrm{Ne} + {}^{208}\mathrm{Pb}$	1.08×10^{-25}	3.84×10^{-19}	21.73	21.14 [22]
HPR	$^{232}\mathrm{U} \rightarrow {}^{82}\mathrm{Ge} + {}^{150}\mathrm{Nd}$	1.02×10^{-33}	1.29×10^{-17}	28.26	–
SF	$^{232}\mathrm{U} \rightarrow {}^{98}\mathrm{Zr} + {}^{134}\mathrm{Te}$	9.57×10^{-31}	7.47×10^{-14}	21.54	21.39 [14]
Alpha (α)	$^{234}\mathrm{U} \rightarrow {}^{4}\mathrm{He} + {}^{230}\mathrm{Th}$	1.68×10^{-10}	7.64×10^{-27}	14.41	12.88 [21]
Cluster	$^{234}\mathrm{U} \rightarrow {}^{26}\mathrm{Ne} + {}^{208}\mathrm{Pb}$	3.08×10^{-28}	8.25×10^{-23}	27.97	25.92 [22]
HPR	$^{234}\mathrm{U} \rightarrow {}^{82}\mathrm{Ge} + {}^{152}\mathrm{Nd}$	1.48×10^{-34}	2.10×10^{-17}	28.90	–
SF	$^{234}\mathrm{U} \rightarrow {}^{100}\mathrm{Zr} + {}^{134}\mathrm{Te}$	9.91×10^{-33}	6.10×10^{-14}	23.62	23.67 [14]
Alpha (α)	$^{236}\mathrm{U} \rightarrow {}^{4}\mathrm{He} + {}^{232}\mathrm{Th}$	8.85×10^{-11}	2.44×10^{-28}	16.19	14.86 [21]
Cluster	$^{236}\mathrm{U} \rightarrow {}^{28}\mathrm{Mg} + {}^{208}\mathrm{Hg}$	6.47×10^{-32}	1.16×10^{-22}	27.80	27.58 [22]
HPR	$^{236}\mathrm{U} \rightarrow {}^{82}\mathrm{Ge} + {}^{154}\mathrm{Nd}$	6.93×10^{-34}	2.08×10^{-17}	29.00	–
SF	$^{236}\mathrm{U} \rightarrow {}^{102}\mathrm{Zr} + {}^{134}\mathrm{Te}$	1.36×10^{-32}	2.63×10^{-14}	23.85	23.89 [14]
Alpha (α)	$^{238}\mathrm{U} \rightarrow {}^{4}\mathrm{He} + {}^{234}\mathrm{Th}$	8.38×10^{-11}	6.62×10^{-30}	17.80	17.14 [21]
Cluster	$^{238}\mathrm{U} \rightarrow {}^{34}\mathrm{Si} + {}^{204}\mathrm{Pt}$	6.99×10^{-32}	2.31×10^{-21}	29.15	29.04 [22]
HPR	$^{238}\mathrm{U} \rightarrow {}^{82}\mathrm{Ge} + {}^{156}\mathrm{Nd}$	7.10×10^{-35}	1.22×10^{-17}	29.45	–
SF	$^{238}\mathrm{U} \rightarrow {}^{106}\mathrm{Mo} + {}^{132}\mathrm{Sn}$	2.43×10^{-32}	5.23×10^{-14}	23.31	23.41[14]

IV. SUMMARY

Summarizing, we have studied 45 cases of spontaneous fission of various parent nuclei, varying from ^{232}U to ^{264}Hs using PCM with spherical choice of decay products. Although PCM was applied earlier for ground state studies such as α decay, cluster emission, and heavy particle radioactivity in the recent past, the same is being used here in reference to spontaneous fission process and its possible competing analysis with other ground state decays such as α, cluster, HPR, etc. Various issues related to shell effects, fine structure and substructure of fission fragments, isospin effect, etc., have been addressed. The reported SF half-lives for all these systems are nicely addressed using PCM calculations performed in the framework of different choices of radius, namely effective sharp radius and Süssmann's central radius. The choice of the most probable decay fragment was identified and the fragments in the mass range $A_2 = 98$–130 (plus complementary heavy fragments) seem to be the prominent contributors towards SF half-lives for all the chosen cases. Apart from this, an attempt was made to explore the decay path of even mass nuclei $^{232-238}$U, in terms of α emission along with most probable cluster decay(s), with a way to identify the magic or near magic daughter(s) in the exotic emission process. Such a study offers two important results: First, the emergence of heavy cluster ^{82}Ge and its corresponding daughter is found equally favored in all the chosen parents independent of mass of parent nucleus, thereby pointing out some future possibilities with such exotic emissions in ground state decay. Second, the behavior of the neck-length parameter indicates that all the individual processes, i.e., α, cluster, and fission occur almost simultaneously in the decay of U isotopes. Such a result could be of interest to investigate various ground state decays and provide new directions for future measurements. As an extension of this work, it will be of further interest to investigate the role of deformations along with appropriate orientations for complete and comprehensive knowledge of SF and heavy cluster dynamics in different mass regions.

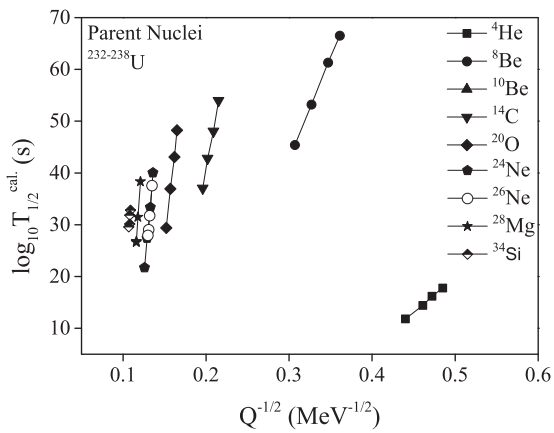

FIG. 11. Geiger-Nuttal plots of $\log_{10}T_{1/2}^{\mathrm{PCM}}$ (s) vs $Q^{-1/2}$ for various clusters emitted from $^{232-238}$U.

ACKNOWLEDGMENTS

Financial support from Department of Science and Technology (DST), New Delhi, India in the form of a major research project (Grant No. EMR/2016/000008) is gratefully acknowledged.

[1] N. Bohr and J. A. Wheeler, Phys. Rev. **56**, 426 (1939); G. N. Flerov and K. A. Petrjak, *ibid.* **58**, 89 (1940).
[2] H. J. Rose and G. A. Jones, Nature (London) **307**, 245 (1984).
[3] A. Sandulescu, D. N. Poenaru, and W. Greiner, Sov. J. Part. Nucl. **11**, 528 (1980).
[4] D. N. Poenaru, R. A. Gherghescu, and W. Greiner, Phys. Rev. Lett. **107**, 062503 (2011).
[5] D. N. Poenaru, R. A. Gherghescu, and W. Greiner, Phys. Rev. C **85**, 034615 (2012).
[6] D. N. Poenaru, M. Ivascu, A. Sandulescu, and W. Greiner, Phys. Rev. C **32**, 572 (1985).
[7] G. Royer, R. K. Gupta, and V. Yu Denisov, Nucl. Phys. A **632**, 275 (1988).
[8] B. Buck and A. C. Merchant, J. Phys. G **15**, 615 (1989).
[9] R. K. Gupta, in *Proceedings of the 5th International Conference on Nuclear Reaction Mechanisms, Varenna*, edited by E. Gadioli (Ricerca Scientifica ed Educazione Permanente, Milano, 1988), p. 416.
[10] S. Kumar and R. K. Gupta, Phys. Rev. C **55**, 218 (1997).
[11] S. S. Malik and R. K. Gupta, Phys. Rev. C **39**, 1992 (1989).
[12] S. K. Arun, R. K. Gupta, S. Kanwar, B. B. Singh, and M. K. Sharma, Phys. Rev. C **80**, 034317 (2009).
[13] D. N. Poenaru and W. Greiner, Phys. Scr. **44**, 427 (1991).
[14] N. E. Holden and D. C. Hoffman, Pure Appl. Chem. **72**, 1525 (2000).
[15] G. Sawhney, M. K. Sharma, and R. K. Gupta, Phys. Rev. C **83**, 064610 (2011).
[16] R. Kumar and M. K. Sharma, Phys. Rev. C **85**, 054612 (2012).
[17] R. Kumar, K. Sandhu, M. K. Sharma, and R. K. Gupta, Phys. Rev. C **87**, 054610 (2013).
[18] G. Sawhney, K. Sandhu, M. K. Sharma, and R. K. Gupta, Eur. Phys. J. A **50**, 175 (2014).
[19] Niyti, G. Sawhney, M. K. Sharma, and R. K. Gupta, Phys. Rev. C **91**, 054606 (2015).
[20] G. Sawhney, K. Sharma, M. K. Sharma, and R. K. Gupta, EPJ Web Conf. **117**, 04013 (2016).
[21] G. Audi, F. G. Kondev, M. Wang, B. Pfeiffer, X. Sun, J. Blachot, and M. MacCormick, Chin. Phys. C **36**, 1157 (2012).
[22] R. Bonetti and A. Guglielmetti, Rom. Rep. Phys. **59**, 301 (2007).
[23] X. Bao, H. Zhang, G. Royer, and J. Li, Nucl. Phys. A **906**, 1 (2013).
[24] H. J. Fink, W. Greiner, R. K. Gupta S. Liran, H. J. Maruhn, W. Scheid, and O. Zohni, in *International Conference on Reactions between Complex Nuclei*, Nashville, 1974, edited by R. L. Robinson *et al.* (North-Holland, Amsterdam, 1975), p. 21.
[25] R. K. Gupta, S. Gulati, S. S. Malik, and R. Sultana, J. Phys. G **13**, L27 (1987).
[26] R. K. Gupta, R. Kumar, N. K. Dhiman, M. Balasubramaniam, W. Scheid, and C. Beck, Phys. Rev. C **68**, 014610 (2003).
[27] M. Balasubramaniam, R. Kumar, R. K. Gupta, C. Beck, and W. Scheid, J. Phys. G **29**, 2703 (2003).
[28] R. K. Gupta, M. Balasubramaniam, R. Kumar, D. Singh, and C. Beck, Nucl. Phys. A **738**, 479c (2004).
[29] G. Audi and A. H. Wapstra, Nucl. Phys. A **595**, 409 (1995).
[30] P. Möller, J. R. Nix, W. D. Myers, and W. J. Swiatecki, At. Nucl. Data Tables **59**, 185 (1995).
[31] R. K. Gupta, R. Kumar, N. K. Dhiman, M. Balasubramaniam, W. Scheid, and C. Beck, Phys. Rev. C **68**, 014610 (2003).
[32] G. Kaur, N. Grover, K. Sandhu, and M. K. Sharma, Nucl. Phys. A **927**, 232 (2014).
[33] R. A. Gherghescu, Phys. Rev. C **67**, 014309 (2003).
[34] R. A. Gherghescu, W. Greiner, and G. Munzenberg, Phys. Rev. C **68**, 054314 (2003).
[35] H. Kröger and W. Scheid, J. Phys. G **6**, L85 (1980).
[36] R. K. Gupta, Phys. Rev. C **21**, 1278 (1980).
[37] S. Yamaji, K. H. Ziegenhain, H. J. Fink, W. Greiner, and W. Scheid, J. Phys. G **3**, 1283 (1977).
[38] S. Yamaji, W. Scheid, H. J. Fink, and W. Greiner, Z. Phys. A **278**, 69 (1976).
[39] M. Greiner and W. Scheid, J. Phys. G **12**, L229 (1986).
[40] G. Süssmann, Z. Phys. A **274**, 145 (1975).
[41] D. N. Poenaru, R. A. Gherghescu, and W. Greiner, Eur. Phys. J. A **24**, 355 (2005).